COMSOL API based Toolbox for the Mixed-Level Modeling of Squeeze-Film Damping in MEMS: Simulation and Experimental Validation

M. Niessner[1,*], G. Schrag[*,1], J. Iannacci[2] and G. Wachutka[1]
[1] Institute for Physics of Electrotechnology, Munich University of Technology, Munich, Germany, [2]MEMS Research Unit, Fondazione Bruno Kessler, Povo di Trento, Italy
*Corresponding author: Martin Niessner, LST TEP, TUM, Arcisstr. 21, 80290 Munich, Germany, niessner@tep.ei.tum.de

Abstract: We present an easy-to-use toolbox for the automated generation of reduced-order mixed-level models for the evaluation of squeeze-film damping in microelectro-mechanical systems. The toolbox is programmed in JAVA and heavily exploits the functionality provided by the COMSOL API. The results obtained from mixed-level model simulation performed in COMSOL Multiphysics agree very well with experimental data. A benchmark of the mixed-level model against other state-of-the-art analytic squeeze-film damping models shows that the mixed-level model is the one with the highest accuracy.

Keywords: MEMS, squeeze-film damping, reduced-order modeling, COMSOL API, experimental validation

1. Introduction

Squeeze-film damping describes the situation when fluid film in a small gap between one moving and one fixed plate (see Fig. 1) exerts viscous damping forces on the moving plate. The viscous forces result from squeezing the fluid out or in across the boundary and, if present, through perforations.

The reliable estimation of squeeze-film damping (SQFD) is a prerequisite for the design of many microelectromechanical systems (MEMS), since the dynamic behavior of most of the latter is dominated by SQFD exerted by the air in the gap between the moving microstructures and the substrate. The proper operation of some MEMS devices does even depend crucially on the specific magnitude of total viscous damping force, i.e. the pressure level within the hermetically sealed package [1].

Commonly, the analytical models presented by Bao *et al.* [2] and Veijola [3] are used for the calculation of SQFD in MEMS, even though a systematic experimental validation of these models was not available for several years. Only recently, Veijola *et al.* [4] and De Pasquale *et al.* [5] presented first experimental evaluations of these models at normal pressure. The error for some of the devices investigated in these evaluations exceeded 63%.

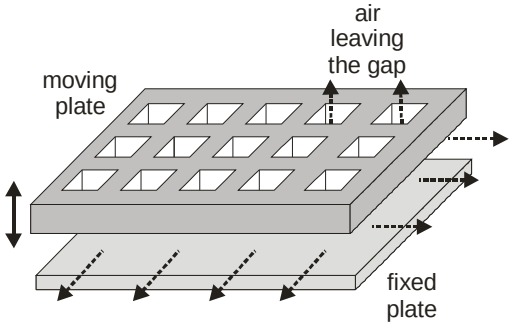

Figure 1. Illustration of a SQFD-dominated geometry: a suspended perforated plate is vibrating above a fixed plate. Due to this motion, the fluid in the gap between the plates enters and leaves across the boundary and through the perforation holes.

These high errors are due to the fact that SQFD is, by its nature, a distributed effect that cannot be simply lumped into a single analytical model. Moreover, SQFD is a strongly fluid-mechanically coupled problem, i.e. not only the fluidic, but also the mechanical domain needs to be modeled accurately.

These findings prompted us to investigate the potential of an alternative model for the calculation of SQFD, namely the mixed-level model (MLM), as suggested in [6,7]. The general idea of the MLM is to evaluate the Reynolds equation where applicable, using a spatially discretized flux-conserving finite network, and to employ lumped physics-based fluidic resistors to account for holes and the pressure drop along the boundaries.

This concept also explains the prefix "mixed-level": the Reynolds equation is evaluated using a spatial discretization ("distributed level") and complemented with

lumped fluidic resistors, i.e. single analytic equations ("concentrated or compact level").

2. General Workflow

In order to make the mixed-level modeling approach as easy and as fast to use as possible, we implemented an automated model generation toolbox in JAVA that exploits the API functionality provided from COMSOL Multiphysics Version 4 on (see workflow in Fig. 2).

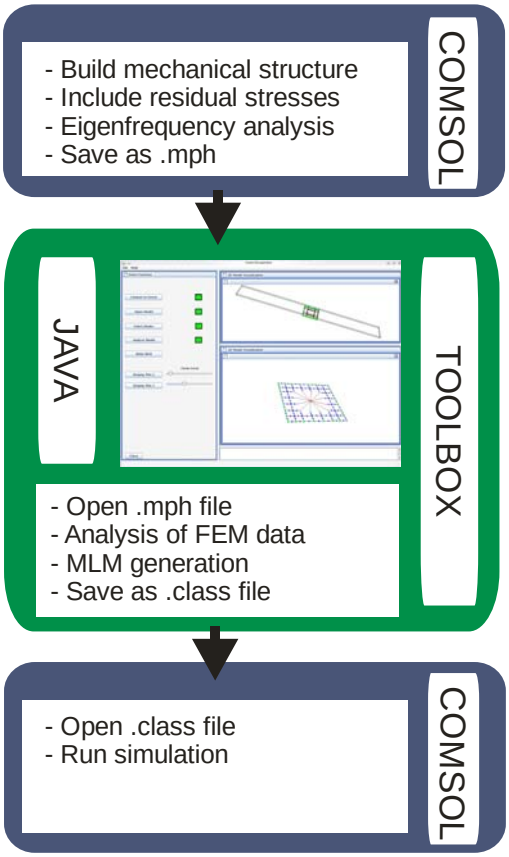

Figure 2. General workflow of the generation and simulation of MLMs using the toolbox.

The procedure starts with a pure mechanical model of the MEMS structure built directly in COMSOL Multiphysics. After performing an eigenfrequency analysis of the mechanical model in COMSOL Multiphysics, the model as well as the results are saved as standard .mph file.

The .mph file is then opened in the JAVA-based toolbox, which automatically analyzes the features of the MEMS structure (see section 4 for details), generates the fluid-mechanically coupled MLM and saves the MLM in a standard .class file.

Finally, opening the .class file in COMSOL Multiphysics automatically implements all equations of the MLM, a set of coupled ordinary differential equations with usually between 100 and 4000 degrees of freedom, as General Equation objects making the MLM ready for simulation in COMSOL Multiphysics.

3. Governing Equations

The modal superposition technique [8] is used to derive a reduced-order mechanical model of the MEMS structure based on the eigenfrequencies ω_i and eigenmodes $\overline{\theta}_i$ obtained from the mechanical eigenfrequency analysis performed in COMSOL Multiphysics. This modal mechanical model enables taking the dynamic deformation of the structure into account whilst SQFD is evaluated. The modal equation of motion for one eigenmode reads:

$$\ddot{q}_i + \omega_i^2 q_i = \overline{\theta}_i^T \overline{F}_{ext} \qquad (1)$$

Here, q_i and ω_i denote the amplitude and the frequency of the i-th eigenmode. $\overline{\theta}_i$ denotes the vector of the discretized shape of the i-th eigenmode. $\overline{\theta}_i$ is normalized w.r.t. the mass matrix. $\overline{F}_{ext}$ denotes the vector of the external forces acting on the MEMS structure such as electrostatic, viscous damping and contact forces. The number of eigenmodes needs to be chosen according to the desired accuracy of the mechanical model.

Assuming laminar flow and that the lateral dimensions of the MEMS structure are much larger than the vertical gap width, the Reynolds equation [9] is used for the modeling of the SQFD exhibited by the surrounding atmosphere:

$$\nabla\left(\frac{\rho h^3}{12\eta}\nabla p\right) = \frac{\partial}{\partial t}(\rho h) \qquad (2)$$

Here, ρ denotes the density of the surrounding gas, η the viscosity of the gas, h the local gap height and p the local pressure. For the implementation of eq. 2 in the toolbox, we assumed the gas to be incompressible (see eq. 3).

$$\frac{\partial}{\partial t}\rho = 0 \qquad (3)$$

This leads to a incompressible but still nonlinear Reynolds equation:

$$\nabla\left(\frac{h^3}{12\eta}\nabla p\right)=\frac{\partial h}{\partial t} \qquad (4)$$

Eq. 4 is evaluated using a finite network [6,7], i.e. eq. 4 is spatially discretized using the mesh of the mechanical model or another one in order to obtain the pressure profile in the gap between the moving and the fixed plate. It is important to point out that finite networks are very different from finite elements. Finite networks primarily use a flux-conserving discretization scheme employing generalized Kirchhoffian network theory as a framework. Thus, finite networks do not use ansatz functions, but Kirchhoffian network elements to discretize the equation of interest on the mesh. The result is a Kirchhoffian network governed by across and through variables. In case of the finite fluidic network used for evaluating the Reynolds equation, the across and through variables are the pressure difference and the volume flow rate between two adjacent nodes.

In terms of its Kirchhoffian network representation, the left hand side of eq. 4 results in a nonlinear fluidic resistor that models the flow of fluid between two nodes (see eq. 5) and the right hand side of eq. 4 results in a fluidic source (see eq. 6) that models the flow of air due to the displacement of the moving membrane:

$$Q_{kl}=G_{kl}\cdot p_{kl}=\frac{w_{kl}\cdot(h_{kl})^3}{12\eta\cdot d_{kl}}\cdot\psi_{R}\cdot p_{kl} \qquad (5)$$

$$Q_{S,k0}=A_k\cdot\dot{h}_k \qquad (6)$$

Here, Q_{kl}, G_{kl} and p_{kl} denote the flow rate, conductance and pressure difference between two adjacent nodes k and l of the network. w_{kl}, h_{kl} and d_{kl} denote the width, height and length of the Poiseuille flow channel between two adjacent nodes. ψ_R denotes a correction for gas rarefaction effects taken from Veijola and are also listed in [10] and [11]. $Q_{S,k0}$ denotes the flow rate resulting from the fluidic source at the k-th node. A_k and $\dot{h}_k$ denote the nodal area and nodal velocity at the k-th node.

Using a finite network for the spatially distributed evaluation of the nonlinear Reynolds equation has two essential advantages. First, perforation holes and effects along the boundary, that are not accounted for in the Reynolds equation in its original form, can be easily taken into account using lumped models formulated in terms of across and through variables that are attached to the respective nodes of the finite network. Second, the gap width does not have to be constant from node to node, but may vary. This is very useful if non-uniform gap widths and/or the dynamic mechanical deformation of the MEMS structure have to be taken into account.

The aforementioned pressure drop along the boundary is modeled by physics-based fluidic resistors that are attached to every node located at the boundary of the structure. The boundary resistance $R_{B,k}$ of the k-th node reads [10,11]:

$$R_{B,k}=0.84\frac{3\pi\eta}{(h_k)^2 b_k}\cdot\psi_{BT}^{-1} \qquad (7)$$

Here, b_k and ψ_{BT} denote the length of the boundary associated with the k-th node and a correction for gas rarefaction effects [10,11].

Each hole is modeled by a series of three fluidic resistors. The resistor $R_{T,r}$ accounts for the transition of the flow from the gap into the hole, the resistor $R_{C,r}$ accounts for the fluidic resistance of the hole channel and $R_{O,r}$ accounts for the resistance of the orifice of the r-th perforation hole [10,11]:

$$R_{T,r}=0.84\frac{3\pi\eta}{(h_r)^2 b_r}\cdot\psi_{BT}^{-1} \qquad (8)$$

$$R_{C,r}=\frac{12\eta L_r}{0.42(s_r)^4}\cdot\psi_{C}^{-1} \qquad (9)$$

$$R_{O,r}=\frac{21\eta}{(s_r)^3}\cdot\psi_{O}^{-1} \qquad (10)$$

Here, h_r, s_r, b_r and L_r denote the gap width at the r-th hole, the side length of the square hole, its perimeter and its channel length. ψ_C and ψ_O denote corrections for gas rarefaction [10,11].

For the purpose of illustration, Fig. 3 shows the fluidic network with lumped element models attached for a square plate with a single square perforation hole.

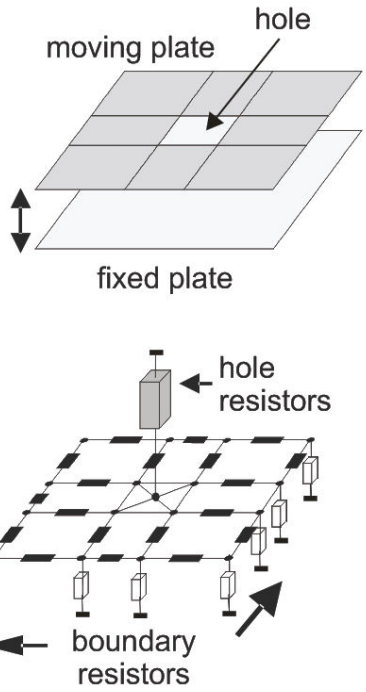

Figure 3. Illustration of the finite network model with lumped models attached using the example of a membrane with only one perforation. Black 2D-boxes symbolize the finite network and 3D-boxes the lumped resistors along the boundary and at the hole.

The coupling between the fluidic and mechanical domain is bi-directional and realized through the changing gap widths h_k (see eq. 11) and the nodal damping forces $F_{damp,k}$ (see eq. 12) that are obtained from multiplying the nodal pressures p_k with the nodal areas A_k:

$$h_k = h_k\left(\bar{q}\right) = h_{0,k} + \sum_i \phi_{i,k} \cdot q_i \qquad (11)$$

$$F_{damp,k} = p_k \cdot A_k \qquad (12)$$

Here, $\bar{q}$ and $h_{0,k}$ denote the vector of modal amplitudes and the initial local gap width at the k-th node. Using the vector $\bar{F}_{damp}$ of all nodal damping forces, eq. 1 now reads:

$$\ddot{q}_i + \omega_i^2 q_i = \bar{\theta}_i^T \left(\bar{F}_{damp} + \bar{F}_{ext}\right) \qquad (13)$$

4. Automated Model Generation Toolbox

Fig. 4 shows the graphical user interface (GUI) of the JAVA-based toolbox. The left section of the GUI consists of buttons that enable the user to open a .mph file, to select an appropriate number of eigenmodes, to run the model analysis, to generate and to save the fluid-mechanically coupled MLM. The right section of the GUI features two panels that display the analyzed topography of the MEMS structure and visualize the resulting MLM.

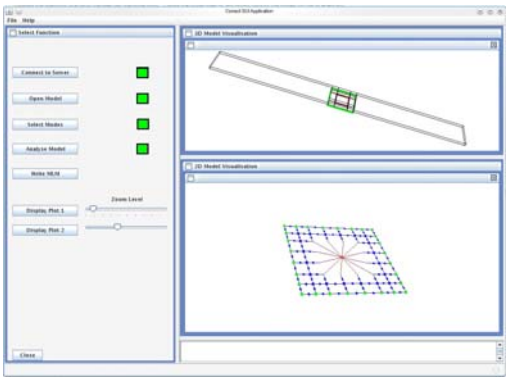

Figure 4. View of the GUI of the JAVA-based toolbox that exploits the functionality offered by the COMSOL API.

The algorithms that automatically recognize the topography of the structure and that automatically generate the MLM are the essential features of the toolbox (see Fig. 5).

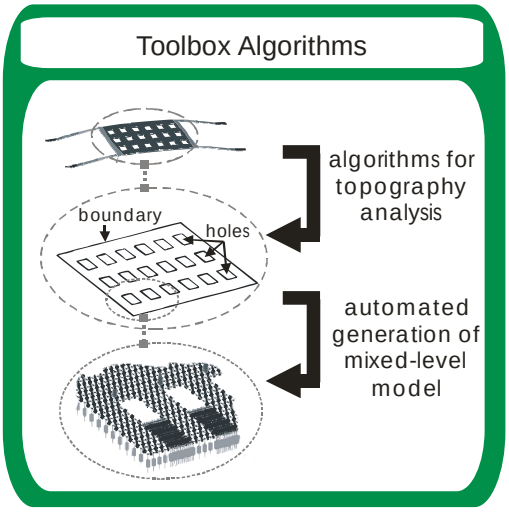

Figure 5. Illustration of the algorithms implemented in the JAVA-based toolbox.

5. Results

The SQFD on various structures was analyzed both, numerically using MLMs and by measurement. Simulation and measurement were compared by evaluating the quality

factor. For the simulations, the quality factor was extracted from the envelope of the damped oscillation in the time domain. For the measurements, the quality factor was extracted from the frequency domain using the 3dB-bandwith method. The experimental setup for the measurements consisted of a Polytec MSA-500 scanning laser Doppler vibrometer and a specifically developed pressure chamber with electronic pressure control (see Fig. 6).

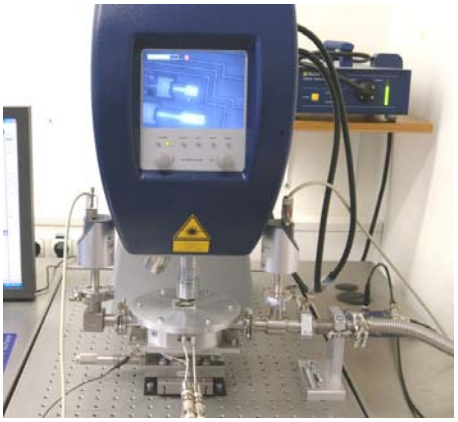

Figure 6. Experimental setup consisting of a Polytec MSA-500 and a specially developed pressure chamber with pressure control.

For the sake of clarity, we will present only the results of one MEMS resonator and one radio frequency MEMS switch (RF-MEMS switch) in this paper. The technical details of the two devices are given in Table 1.

Figs. 7 and 8 show the measured and simulated pressure-dependent quality factors of the two devices. The graphs indicate that an additional dissipative mechanism dominates the damping behavior of these structures at pressures lower than approx. 100 mbar and limits the quality factors in this regime. This is taken into account by calculating a quality factor Q_{TOTAL} from the simulated quality factor Q_{MLM} and a value Q_{LIMIT} extracted at minimum pressure:

$$\frac{1}{Q_{Total}} = \frac{1}{Q_{MLM}} + \frac{1}{Q_{LIMIT}} \qquad (14)$$

At normal pressure, the measured and simulated quality factors using the MLM show very good agreement, i.e. the relative error does not exceed 7%. The MLMs furthermore show reasonable agreement down to pressures of about 100 mbar.

	Device	
	Resonator (Fig.7)	*Switch (Fig. 8)*
Material	Silicon	Gold
Membrane width [µm]	139	140
length [µm]	133	260
thickness [µm]	15	5
Specified gap [µm]	2	3
Hole side length [µm]	13.3	20
Number of holes	7 x 7	3 x 6
Perforation level [%]	46.9	23
Resonance frequency [kHz]	44	15

Table 1. Technical data of the two investigated MEMS devices.

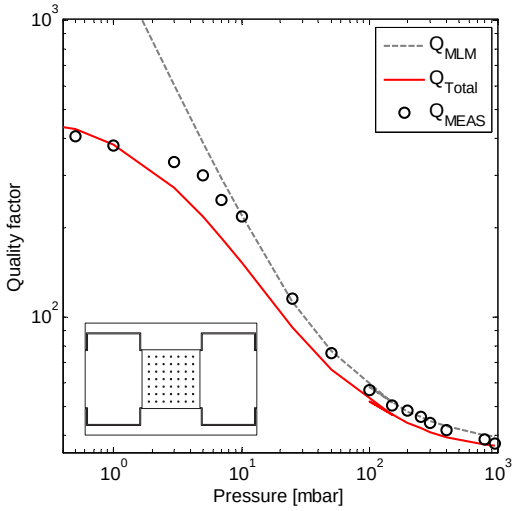

Figure 7. Measured and simulated quality factors of the MEMS resonator. Q_{MEAS} denotes the measured quality factor, Q_{MLM} the quality factor obtained from MLM simulation and Q_{TOTAL} the quality factor from eq. 14.

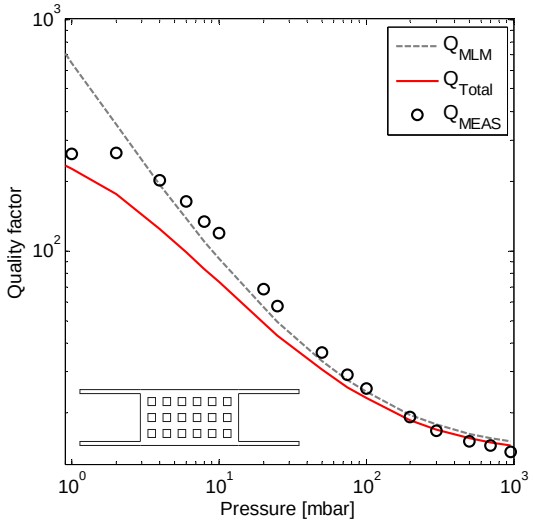

Figure 8. Measured and simulated quality factors of the RF-MEMS switch.

6. Discussion

The simulated results and the measured data agree very well when compared to the models by Bao *et al.* [2] and Veijola [3] that show errors exceeding 25% already at normal pressure (see Table 2).

	Resonator	RF switch
Q_{MEAS}	37.47	13.58
$Q_{TOTAL,MLM}$	36.72 (+2%)	14.49 (-6.7%)
$Q_{TOTAL,BAO}$ [2]	23.77 (+36.6%)	6.84 (+49.6%)
$Q_{TOTAL,VEIJOLA}$ [3]	22.32 (+40.4%)	17.16 (-26.3%)

Table 1. Measured and calculated quality factors at normal pressure of the two devices. All the calculated quality factors include the limiting damping mechanism through Q_{LIMIT}. The relative error is also given within brackets.

We attribute the better agreement of the MLM to its ability to take accurately into account the actual topography of the MEMS structure by means of its finite network and locally attached lumped resistors. Especially the RF-MEMS switch is very difficult to handle with analytic compact models because it has a very non-uniform gap [11].

The SQFD-limited quality factor of one more MEMS resonator has been simulated and compared with pressure-dependent measured data in [12]. The MLM shows an equivalent high accuracy. Moreover, the MLM has been evaluated for SQFD-damped cantilevers and clamped-clamped beams and showed again equivalent high accuracy. Unfortunately, due to restrictions from our project partner, we are not allowed to publish these results.

In [12], the MLM is also benchmarked against the mixed-mode SQFD model presented by Veijola and Raback [13]. The model presented in [13] is implemented in COMSOL 3.5a and follows the same idea as the MLM, but using the finite element method. The benchmark presented in [12] shows that the MLM performs also better than the model presented in [13]. We believe that the better performance of the MLM is due to the nature of the models employed to account for effects along the boundary and the perforation holes. For instance, the model correcting for the pressure drop along the boundary is a physics-based model in the case of the MLM, whereas the model used in [13] is a heuristic one.

The issue that has yet to be addressed is the behavior of the MEMS structures at pressures lower than 100 mbar. The limiting damping mechanisms in this regime have to be identified in order to enable an evaluation of the corrections for gas rarefaction listed in [10,11] and used in eqs. 5 and 7-10.

7. Conclusion

The very good agreement of the experimental data and the results from mixed-level model simulations at normal pressure is a remarkable result and demonstrates the accuracy and the predictive power of our transparent and physics-based approach.

In particular, the mixed-level modeling approach outperforms the analytic model by Bao *et al.* [2] and Veijola *et al.* [3,13].

The JAVA-based toolbox, which enables the easy and fast generation of mixed-level models, makes our modeling methodology directly accessible to the large community of MEMS designers.

8. Outlook

Possibilities for improvement are the extension to compressible fluids and a frequency domain formulation of the MLM, so that the quality factor of a MEMS structure can also be quickly evaluated using complex eigenvalue analysis.

Moreover, already available algorithms [14] that automatically reduce the MLM if many perforation holes and, thus, many degrees of freedom are present, could be implemented.

9. References

1. R. Khalilyulin, T. Steinhuber, *et al.*, "Hardware/Software Co-Simulation for the Rapid Prototyping of an Acceleration Sensor System with Force-Feedback Control", *Proc. of the 40th European Solid-State Device Research Conf.*, ESSDERC 2010, Spain, pp. 186-189 (2010).

2. M. Bao, H. Yang, *et al.*, "Modified Reynolds' equation and analytical analysis of squeeze-film air damping of perforated structures", *J. Micromech. Microeng.*, **13**, pp. 595-800 (2003).

3. T. Veijola, "Analytic damping model for an MEM perforation cell", *J. Microfluid Nanofluid*, **2**, pp. 249-260 (2006).

4. T. Veijola, G. De Pasquale, *et al.*, "Experimental validation of compact damping models of perforated MEMS devices", *J. Microsystem Tech.*, **15**, pp. 1121-1128 (2009).

5. G. De Pasquale, T. Veijola, *et al.*, "Modelling and validation of air damping in perforated gold and silicon MEMS plates", *J. Micromech. Microeng.*, **20**, pp. 015010(12) (2010).

6. G. Schrag, P. Voigt, *et al.*, "Physically-based modeling of squeeze film damping by mixed level system simulation", *Digest Tech. Papers of Transducers'01*, TRANSDUCERS 2001, Germany, pp. 670-673 (2001).

7. G. Schrag, G. Wachutka, "Physically based modeling of squeeze film damping by mixed-level system simulation", *Sensors and Actuators A*, **97-98**, pp. 193-200 (2002).

8. L. Gabbay, J. Mehner, *et al.*, "Computer-aided generation of reduced-order dynamic macromodels - I: Geometrically linear motion", *J. Microelectromechanical Systems*, **9**, pp. 262–269 (2000).

9. B. Hamrock, *"Fundamentals of Fluid Film Lubrication"*. McGraw-Hill, Singapore (1994).

10. R. Sattler, *"Physikalisch basierte Mixed-Level Modellierung von gedämpften elektromechanischen Systemen"*, Shaker Verlag, Aachen, 2007.

11. M. Niessner, G. Schrag, *et al.*, "Macromodel-based simulation and measurement of the dynamic pull-in of viscously damped RF-MEMS switches", *Sensors and Actuators A*, in press and already available online.

12. M. Niessner, G. Schrag, *et al.*, "Mixed-level modeling of squeeze film damping in MEMS: simulation and pressure-dependent experimental validation", *Digest Tech. Papers of Transducers'11*, TRANSDUCERS 2011, China, pp. 1693-1698 (2011).

13. T. Veijola, P. Raback, "Methods for solving gas damping problems in perforated microstructures using a 2D finite-element solver", *J. Sensors*, **7**, pp. 1069-1090 (2007).

14. M. Niessner, G. Schrag, *et al.* , "Reduced-Order Modeling and Coupled Multi-Energy Domain Simulation of Damped Highly Perforated Microstructures", *Proc. of the 8th Congress on Computational Mechanics and the 5th European Congress on Computational Mechanics in Applied Sciences and Engineering*, WCCM8/ECCOMAS 2008, Italy, 2 pages (2008).